


Wave-function reconstruction for large phase gradients based on optical differentiationYonghang Lu, Junfan Zhu, Fuhua Gao,^{*} and Zhiyou Zhang[†]
College of Physics, Sichuan University, Chengdu 610064, China (Received 20 June 2023; revised 8 January 2024; accepted 9 January 2024; published 31 January 2024)

The wave function is the cornerstone of quantum theory, and various techniques have been proposed for its direct measurement. The reconstruction of the wave function can be achieved by utilizing the real and imaginary components of momentum weak value, which correspond to amplitude and phase differentiation, respectively. However, these methods are limited in their applicability to wave functions with large phase gradients due to the weak coupling condition, which is a fundamental constraint. In this paper, we propose a method for reconstructing wave functions with large phase gradients based on optical differentiation through weak measurement. We have developed a more generalized theory of phase differentiation and implemented a common optical path and fast measurement for wave functions with large phase gradients. The experimental detection of wave functions with varying phase gradients has validated the reliability of our method. This work expands the range of applications for weak measurement while retaining its high resolution and sensitivity advantages, particularly in the field of wavefront sensing.

DOI: [10.1103/PhysRevA.109.012623](https://doi.org/10.1103/PhysRevA.109.012623)**I. INTRODUCTION**

The wave function, a fundamental concept in quantum mechanics, has attracted a lot of interest of research. As a complex variation, it can be measured indirectly by quantum state tomography through a series of strong measurements and information processing [1,2]. This method requires a large number of measurement processes and it is difficult to realize the simultaneous measurement of the real part (the amplitude) and the imaginary part (the phase) of the wave function. In 2011, Lundeen *et al.* presented a method to directly reconstruct the wave function based on weak measurement [3]. Their scheme uses the real and the imaginary parts of weak value [4,5], corresponding to the wave function's amplitude and phase. However, this method theoretically necessitates an infinitely small pinhole and requires scanning every position to get all the information. In 2015, Shi *et al.* proposed a scheme for directly measuring wave function without scanning [6]. However, the experiment relies on introducing a phase shift to one particular momentum state, which presents significant implementation challenges.

To address these problems, methods of wave-function reconstruction without scanning and manipulating a particular momentum state have been realized [7,8]. Their schemes construct the momentum weak value by controlling different pre- and postselection under weak coupling [9]. Phase differentiation is obtained from the momentum weak value. Although feasible in practice, those schemes have two limitations. First, a sufficiently weak coupling strength is necessary to satisfying the weak coupling condition. Second, the weak

coupling condition requires the momentum uncertainty of the meter wave function to be small as well, which limits the measured wave function to a slow spatial variation. The maximum of phase gradients depends on how weak the coupling strength is.

The complex amplitude in classical theory can be viewed as a wave function when the quantum description of light is not required. Light passing through a substance, such as an optical component or atmospheric turbulence, inevitably induces wavefront distortions. Detection of wavefront distortion enables the measurement of component surface-type and atmospheric turbulence distribution. This method is extensively utilized in surface testing [10] and adaptive optics [11,12]. Moreover, wavefront distortion measurement has facilitated the observation and measurement of transparent organisms or the human eye [13,14]. In these applications, the phase gradient is much larger than the allowable range for weak coupling condition. To apply the method, it is necessary to extend the dynamic range.

Here, we propose an approach for wave-function reconstruction that overcomes the limitations associated with large phase gradients. For the case of small phase gradients, the square of the phase derivative can be measured directly, where three different wave functions modulated by the spatial light modulator (SLM) are measured. For the case of large phase gradients, the differentiation information is wrapped. In this experiment, we measured the phase distribution of collimated light passing through the lenses with a curvature radius of 77.5 mm (focal length $f_1 \approx 15$ cm) and 155.0 mm (focal length $f_2 \approx 30$ cm). Phase differentiation is obtained by solving this wrapped phase (or the square of the phase derivative) with a phase unwrapping algorithm [15–17]. Using the phase differentiation, combined with the difference Zernike polynomial fitting algorithm (DZF) [18,19], the measured phase is reconstructed.

^{*}gaofuhua@scu.edu.cn[†]zhangzhiyou@scu.edu.cn

II. THEORY

The weak coupling condition requires a coupling strength that is extremely weak and it limits the uncertainty of the wave function of the meter. Let us consider a more specific case. The preselected state $|\psi_i\rangle$ is in the state of $1/\sqrt{2}(|H\rangle + |V\rangle)$, where $|H\rangle$ and $|V\rangle$ represent the horizontal and vertical polarization states, respectively. To simplify nomenclature, we use the reduced Planck constant $\hbar = 1$ in the following equations. The evolution operator satisfies $\hat{U} = \exp(-i\gamma\hat{A} \otimes \hat{p})$ [4,20], where γ is the coupling strength, $A = -|V\rangle\langle V|$ is the operator of the polarization, \hat{p} is the operator of momentum. We use the antidiagonal postselected state $|\psi_f\rangle = 1/\sqrt{2}(|H\rangle - |V\rangle)$ and $|x\rangle$ to reach a high sensitivity. The distribution function of the final probability is

$$\begin{aligned} \Phi(x) &= \langle \psi_f | \otimes \langle x | e^{-i\gamma\hat{A} \otimes \hat{p}} | \psi_i \rangle \otimes | \phi \rangle \\ &= \sum_{n=0}^{+\infty} \frac{(-i\gamma)^n}{n!} \langle \psi_f | \hat{A}^n | \psi_i \rangle \langle x | \hat{p}^n | \phi \rangle, \end{aligned} \quad (1)$$

where the pure state wave function $|\phi\rangle = \sum_p \phi_p |p\rangle$ is expanded using the momentum eigenstate $|p\rangle$. The eigenvalue corresponding to the momentum eigenstate $|p\rangle$ is p , and the probability of finding the eigenvalue p is $|\phi_p|^2$. Noting that $\langle \psi_f | \psi_i \rangle = 0$, $\langle \psi_f | \hat{A} | \psi_i \rangle = 1/2$, $\langle \psi_f | \hat{A}^n | \psi_i \rangle = (-1)^{n+1} \langle \psi_f | \hat{A} | \psi_i \rangle$, and $\langle x | \hat{p}^n | \sum_p \phi_p |p\rangle = \sum_p \phi_p p^n \langle x | p \rangle$. Using the formula mentioned above, Eq. (1) can be simplified to obtain

$$\Phi(x) = -\frac{1}{2} \sum_p \phi_p [\exp(-i\gamma p) - 1] \langle x | p \rangle. \quad (2)$$

The significance of Eq. (2) is the key to recovering the wave function, and we find that it has a special meaning under the limitation condition of $|\gamma p| \ll 1$. It should be noted that in our experiments, the coupling strength γ is a constant that is much smaller than the diameter of the wave function, and the restriction on the eigenvalue p is actually a restriction on the wave function. The coupling strength γ is a constant greater than 0, so we get $|p| \ll 1/\gamma$. When the condition of $|p| \ll 1/\gamma$ is satisfied, we can expand Eq. (2) to first order to yield

$$\Phi(x) \approx \frac{-\gamma}{2} \sum_p \phi_p \frac{\partial}{\partial x} \left[\frac{1}{\sqrt{2\pi}} \exp(ipx) \right] = \frac{-\gamma}{2} \frac{\partial}{\partial x} \phi(x), \quad (3)$$

where $\frac{1}{\sqrt{2\pi}} \exp(ipx) = \langle x | p \rangle$, and $\phi(x) = \langle x | \phi \rangle$. Equation (3) shows that when the momentum eigenvalue $|p| \ll 1/\gamma$, the probability distribution function $\Phi(x)$ is the sum of the derivatives of each momentum eigenfunction, or proportional to the derivative of the wave function $\phi(x)$. The previous approach was to use the derivative to recover wave function. However, the derivative of the wave function can only be obtained directly for $|p| \ll 1/\gamma$.

If the momentum eigenvalue of the wave function is arbitrary, it is clear that the previous method is insufficient. In practice, we are more concerned with the amplitude and phase of the wave function, so we express the wave function as $\phi(x) = a(x) \exp[ib(x)]$. For convenience of the writing, we

assume that the amplitude $a(x)$ of the wave function is uniform (when the amplitude $a(x)$ is not uniform, an additional measurement is required to solve it, which is not described here, and readers are referred to the literature [8]). From Eqs. (2) and (3), the detection results are obtained as

$$I(x) = |\Phi(x)|^2 = \frac{a^2}{2} \{1 - \cos[b(x) - b(x - \gamma)]\}. \quad (4)$$

and

$$I(x) = |\Phi(x)|^2 = \frac{a^2}{4} \left[\gamma \frac{\partial b(x)}{\partial x} \right]^2, \quad (5)$$

respectively. Notice that we also give the intensity distribution for the special case $|p| \ll 1/\gamma$. The result of Eq. (5) is proportional to the square of the derivative of the phase. Based on Eq. (5), various methods of edge detection have been developed [21–25]. However, due to the information about phase derivatives less than 0 being hidden, Eq. (5) is not sufficient for reconstructing the wavefront. Similarly, relying on Eq. (4) is also insufficient to reconstruct the wavefront, since there is not a direct relationship between the phase derivative and the intensity distribution. To reconstruct the wavefront, it is necessary to obtain the phase differentiation $\Delta b_x(x) = b(x) - b(x - \gamma)$ from Eq. (4). In Sec. III, we show how to obtain phase differentiation, and how to reconstruct the phase from the phase differentiation.

Let us look at how the condition $|p| \ll 1/\gamma$ changes as the form of the wave function changes. Equation (3) is a special case of Eq. (2) under the condition $|p| \ll 1/\gamma$, so Eq. (5) should be a special case of Eq. (4) under the same condition. Using the condition $|b(x) - b(x - \gamma)| \ll 1$, one can also derive Eq. (5) from Eq. (4), so $|p| \ll 1/\gamma$ and $|b(x) - b(x - \gamma)| \ll 1$ are equivalent to each other. It was mentioned before that γ is a small quantity, so $|b(x) - b(x - \gamma)| \approx |\gamma \frac{\partial b(x)}{\partial x}| \ll 1$. Comparing to the condition $|\gamma p| \ll 1$, it is shown that in the case of uniform amplitude, as the form of the wave function changes, the condition $|p| \ll 1/\gamma$ becomes the condition $|\partial b(x)/\partial x| \ll 1/\gamma$. The experimental setup is shown in Fig. 1. Monochromatic light of wavelength of $\lambda = 632.8$ nm was generated from a He-Ne laser, and defined as propagating along the z axis. A collimated light [to satisfy the condition $a(x, y) = a$] is formed by a filtering system. The filtering system consists of a pinhole and Lens 1 and Lens 2. The collimated light passes through the object to form the measured wave function. The polarizer P1 forms the preselected state $|\psi_i\rangle = 1/\sqrt{2}(|H\rangle + |V\rangle)$. The birefringent crystal (BC) can produce a displacement between ordinary and extraordinary lights, which couples momentum and polarization [26]. This displacement is the coupling strength γ . The action of the BC represents the evolutionary operator $\hat{U} = \exp(-i\gamma\hat{A} \otimes \hat{p})$. Rotating BC around the z axis can change the coupling direction to obtain the phase differentiation in any direction. The polarizer P2 controls the postselected state $|\psi_f\rangle = 1/\sqrt{2}(|H\rangle - |V\rangle)$. The $I(x, y)$ is imaged by Lens 3 and recorded by a charge-coupled device (CCD). To complete the first set of experiments, the object in the optical path was replaced by an SLM loaded with a weak phase. For the second set of experiments, we replaced the object with two lenses, which generated two wave functions with large phase gradients.

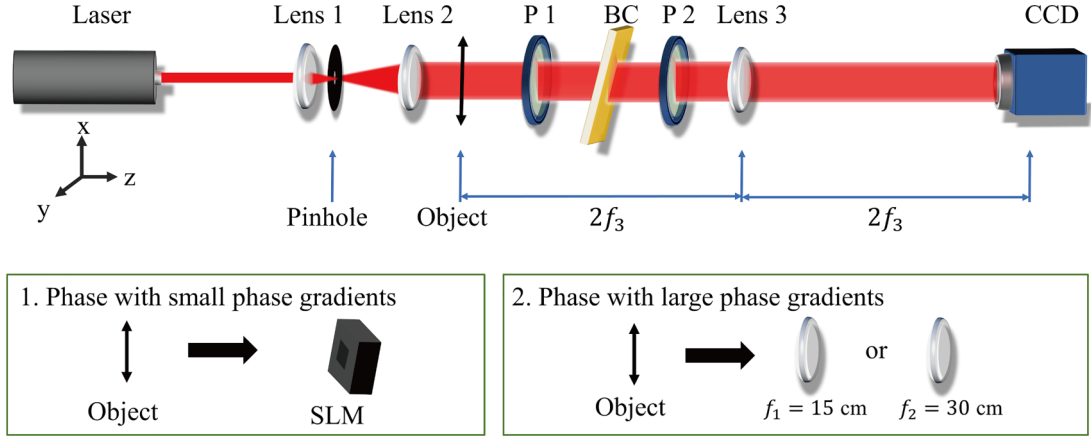


FIG. 1. Experimental setup. The He-Ne laser generates a Gaussian beam with a wavelength of 632.8 nm, which passes through a filtering system consisting of the pinhole and Lens 1 and Lens 2 to form a collimated light. The collimated light incident on the object forms the wave function to be measured. The polarizers P1 and P2 are used to set pre- and postselected states, respectively. The birefringent crystal (BC) couples polarization and momentum. Finally, the $I(x, y)$ is imaged by Lens 3 into a plane, where a charge-coupled device (CCD) is placed to obtain the light intensity. The SLM loaded with the phase of small gradients instead of the object completes the first set of experiments. For the second set of experiments, object was replaced with a lens with a focal length of 15 cm or 30 cm, respectively.

III. DATA PROCESSING

We need to further process Eq. (4) to get the phase differentiation $\Delta b_x(x)$. Rewrite Eq. (4) to get

$$\Delta b_x^T(x) = \arccos\left(1 - \frac{2I(x)}{a^2}\right), \quad (6)$$

where T in $\Delta b_x^T(x)$ represents $\Delta b_x^T(x)$ gets wrapped. For example, in Fig. 2(a), wrapped means that the function is compressed between $-\pi/2$ and $\pi/2$. The unknown variable a^2 can be obtained by reading the maximum value of the light intensity distribution. Therefore, the $\Delta b_x^T(x)$ is not the phase differentiation but a wrapped phase. Obtaining phase differentiation from a wrapped phase is called phase unwrapping [15–17]. Since Eq. (4) is an approximation of Eq. (5) at $|p| \ll 1/\gamma$, the phase unwrapping also applies to the case of small phase gradient.

The general one-dimensional phase unwrapping can be achieved by compensating a value of π in each phase jump as

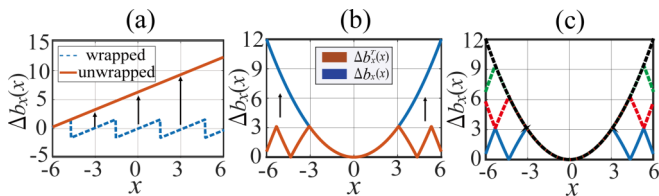


FIG. 2. The phase unwrapping algorithm. (a) The general one-dimensional (1D) phase unwrapping. The process can be viewed as increasing π at $(-6, 3\pi/2)$, increasing 2π at $(-\pi/2, \pi/2)$, and so on. The compensation value is an integer multiple of π . (b) The phase unwrapping for $\Delta b_x^T(x)$. Unlike the general method, the compensation value is not a constant, as shown in the figure. (c) The unwrapping process from $\Delta b_x^T(x)$ to $\Delta b_x(x)$. Starting at $x = 0$, when the point $\Delta b_x^T(x) = \pi$ is encountered (the point is $x = 3.07$ or $x = -3.07$), the function is flipped in the domain of definition of $(3.07, 6)$ or $(-6, -3.07)$. Continue to look for $\Delta b_x^T(x) = 2\pi$ and repeat the above process.

shown in Fig. 2(a). The same approach can be used in the 2D phase [16,17]. Unlike the general approach, the compensation value of the wrapped phase $\Delta b_x^T(x)$ is not $n\pi$, where n is an integer. As shown in Fig. 2(b), to obtain $\Delta b_x(x)$ from $\Delta b_x^T(x)$, the compensation value is not constant. We take $\Delta b_x(x) = 1/3 \times x^2$ as an example to illustrate the process of getting $\Delta b_x(x)$ from $\Delta b_x^T(x)$. This process is shown in Fig. 2(c): starting at $x = 0$, when the point $\Delta b_x^T(x) = \pi$ is encountered (the point is $x = 3.07$ or $x = -3.07$), the function is flipped in the domain of definition of $(3.07, 6)$ or $(-6, -3.07)$. After that the function becomes the red dashed line in Fig. 2(c). Continue to look for $\Delta b_x^T(x) = 2\pi$ (the point is $x = 4.34$ or $x = -4.34$) and flipping the function again in the domain of definition $(4.34, 6)$ and $(-6, 4.34)$. Keep repeating the process of flipping the function until we get $\Delta b_x(x)$. In summary, the phase differentiation can be obtained by constantly flipping the function in different domains of definition.

The measured phase is reconstructed by bringing the phase differentiation of two orthogonal directions into the DZF [18,19]. In the following, we discuss the DZF in detail. The original phase is reconstructed and written as

$$b(x, y) = \sum_{i=1}^{(k+1)(k+2)/2} c_i z_i(x, y), \quad (7)$$

where $z_i(x, y)$ represents the i th term of the Zernike polynomial [27], and c_i is the coefficient of the i th Zernike polynomial. The letter k refers to the order of the polynomial, and the summation limit is $(k+1)(k+2)/2$. A higher value of k corresponds to greater precision in the fitting procedure. In this context, c_i is the value to be obtained. The phase differentiation can be decomposed as

$$\Delta b_x(x, y) = \sum_{i=1}^{(k+1)(k+2)/2} c_i [z_i(x, y) - z_i(x - \gamma, y)] \quad (8)$$

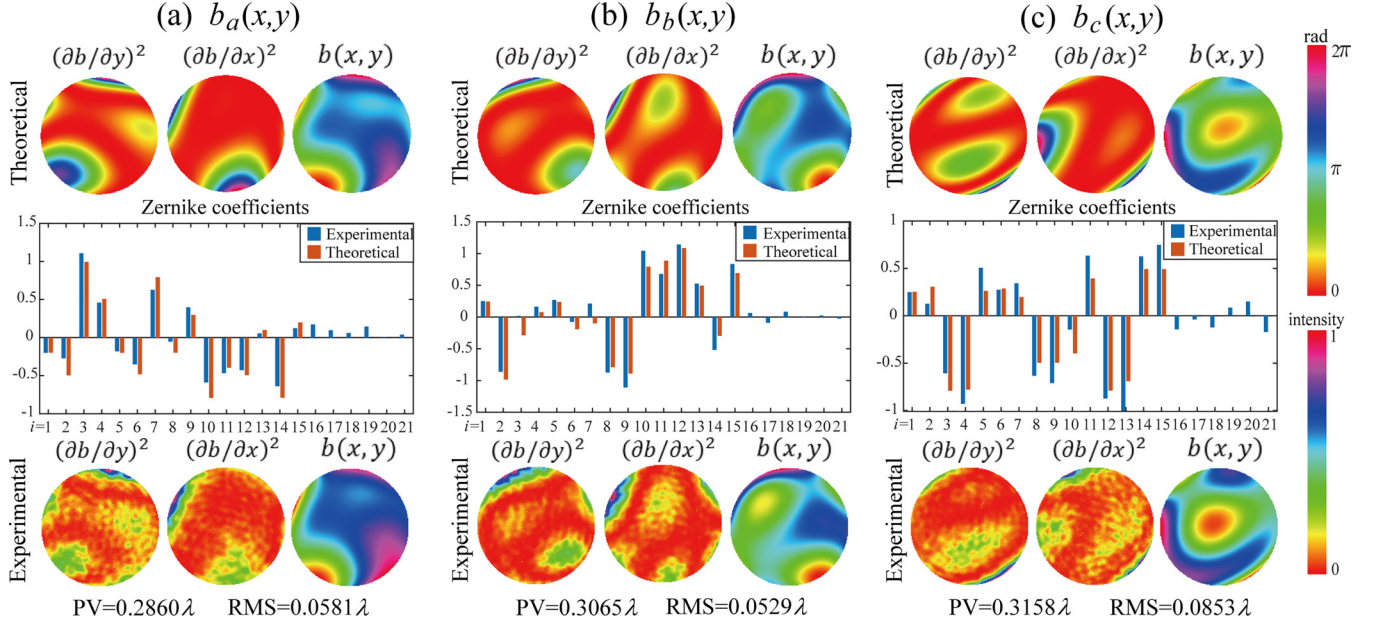


FIG. 3. Experimental results for small phase gradients. The three wave functions $b_a(x, y)$, $b_b(x, y)$, and $b_c(x, y)$ are formed using the first 15 Zernike polynomials and loaded into the SLM. The theoretical $(\partial b/\partial y)^2$, $(\partial b/\partial x)^2$ and phase distributions, Zernike coefficients, and experimental $(\partial b/\partial y)^2$, $(\partial b/\partial x)^2$, and phase distributions are shown. Finally, the peak-to-valley (PV) and root-mean-square (RMS) values of the recovery error were calculated and the unit is the wavelength λ of the incident light.

and

$$\Delta b_y(x, y) = \sum_{i=1}^{(k+1)(k+2)/2} c_i [z_i(x, y) - z_i(x, y - \gamma)]. \quad (9)$$

Rewriting Eqs. (8) and (9) into matrix form, we get

$$\begin{pmatrix} \Delta b_x(x, y) \\ \Delta b_y(x, y) \end{pmatrix} = C \begin{pmatrix} \Delta z_x(x, y) \\ \Delta z_y(x, y) \end{pmatrix}, \quad (10)$$

where $\Delta z_x(x, y) = z_i(x, y) - z_i(x - \gamma, y)$, $\Delta z_y(x, y) = z_i(x, y) - z_i(x, y - \gamma)$, and C is the Zernike coefficient matrix of the original phase. The coefficients can be obtained by solving the matrix equation by the least-squares method.

IV. RESULTS

In the first experiment, we verify the correctness of Eq. (5), which states that for weak phase, the detection result is proportional to the square of the phase derivative. We measured three phases consisting of the first 15 [$k = 4$ in Eq. (7)] Zernike polynomials. The phase distribution is a circle that is the inscribed circle of a 214×214 pixels rectangle on the SLM, and the diameter of the circle is 1498 \AA . The experimental coupling strength γ is 0.1 mm, and $|b(x) - b(x - \gamma)| \leq 0.15 \text{ rad}$. The values of theoretical $(\partial b/\partial y)^2$, $(\partial b/\partial x)^2$ and the phase distributions, the Zernike coefficients, and the experimental values of $(\partial b/\partial y)^2$, $(\partial b/\partial x)^2$ and phase distributions are shown in Fig. 3. In order to judge the experimental value of $b(x, y)$, we calculated the root-mean-square (RMS) and peak-to-valley (PV) values of their differences between the theoretical value and its, as in the bottom of Fig. 3. Since the reconstruction accuracy is related to the wavelength of the incident light, we take the unit as λ . Notice that the detection results in Fig. 3 are the square of the derivative of the phase,

and using the phase unwrapping the phase differentiation can be obtained (not plotted in the Fig. 3) from the detection result.

For weak phase, we want the detection result of the CCD to be proportional to the square of the phase derivative and the reconstructed phase to be the same as the phase on the loaded SLM. As can be seen in Fig. 3, for any one of the three wavefronts, the experimental values of $[\partial b/\partial y(x)]^2$ and the theoretical values of $[\partial b/\partial y(x)]^2$ are very similar. From the RMS values, the average value of absolute error is about 0.06λ (38 nm), and the relative error is about 6% (the maximum loading phase of the SLM is 2π , which is converted to length representing one wavelength, so the relative error is $0.058\lambda/\lambda$). It shows that Eq. (5) and the phase unwrapping are correct.

In the second set of experiments, we verified that the method still works under the large phase gradients. The object in Fig. 1 is replaced by the planoconvex lenses with a curvature radius of 77.5 mm ($f_1 \approx 15 \text{ cm}$) and 155.0 mm ($f_2 \approx 30 \text{ cm}$), respectively. Here, f_1 and f_2 represent the focal lengths of the lenses. The aperture of the measurement area is 4.8 mm. The maximum values of $|b(x) - b(x - \gamma)|$ for the two measured wave functions are 15.8 rad and 7.7 rad, respectively. Under the condition of the large phase gradients, the phase differentiation is wrapped. The detection result $I(x, y)$ for the lens with $f_1 = 15 \text{ cm}$ is shown in Fig. 4(a). According to Eq. (6), the wrapped phase $\Delta b_y^r(x, y)$ is calculated using detection result $I(x, y)$, and then the phase unwrapping is used to obtain the phase differentiation $\Delta b_y(x, y)$. We show the process of solving for $\Delta b_y(x, y)$ in Fig. 4(b) with a column of data for $x = 0$. The distribution of the phase differentiation $\Delta b_y(x, y)$ is shown in Fig. 4(c). Figures 4(d)–4(f) correspond to the data processing of the lens with $f_2 = 30 \text{ cm}$. In this experiment, since the measured object is a spherical lens, the measured phase can be viewed as

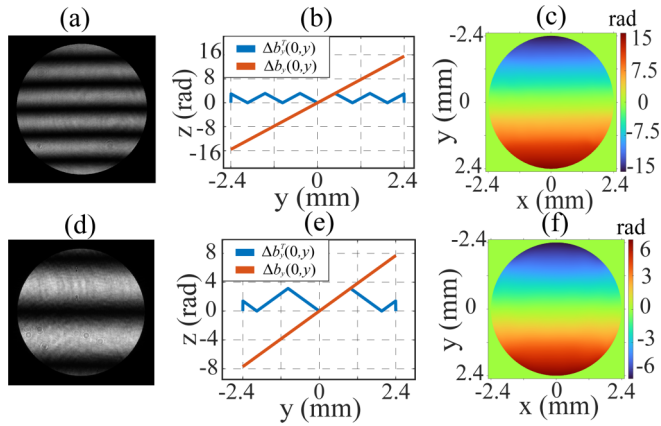


FIG. 4. The phase unwrapping for large phase gradients. (a)–(c) correspond to the data processing of the lens with $f_1 \approx 15$ cm. (d)–(f) correspond to the data processing of the lens with $f_2 \approx 30$ cm. The x axis and y axis represent the aperture of the measured phase, and the z axis and the color bar characterize the size of the phase. (a) and (d) The detection result $I(x, y)$ of CCD. (b) and (e) The process of phase unwrapping of the center column. (c) and (f) The phase differentiation.

a sphere, and its phase differentiation should be a tilted plane. Figures 4(c) and 4(f) are also inclined planes and are considered to be correct. Their correctness is further verified in the reconstructed phase.

We obtain the phase differentiation Figs. 4(c) and 4(f) (only one direction is drawn in to a wavefront) under the condition of the large phase gradients. Using the DZF, we calculated $b(x, y)$, as in Fig. 5(a). To illustrate the correctness of the results, we calculated the theoretical phase distribution $b_1(x, y)$. The theoretical value $b_1(x, y)$ can be acquired by multiplying the optical path difference (OPD) by $k = 2\pi/\lambda$. The reconstructed accuracy Fig. 5(b) is expressed by the difference between the reconstructed result $b(x, y)$ and $b_1(x, y)$. The PV and RMS values of the reconstructed accuracy corresponding to the two lenses are about 1.44λ (9.05 rad) and 0.27λ (1.70 rad), 0.50λ (3.14 rad), and 0.12λ (0.75 rad), respectively. The RMS value is only about 1% of the phase distribution $b(x, y)$. This means that the experimental values are very close to the theoretical values. This conclusion can be seen more intuitively in Fig. 5(c), which plots the cross section of the theoretical and experimental values.

For each measured wave function there is a region under weak coupling. In Figs. 4(a) and 4(d), for example, the dark stripes in the center are considered under the approximation condition of weak coupling, and the wave function with large curvature has a small weak coupling region. A common technology in surface testing is the lateral-shear interferometer [27], which also goes through phase unwrapping and reconstructing. However, our method requires only one

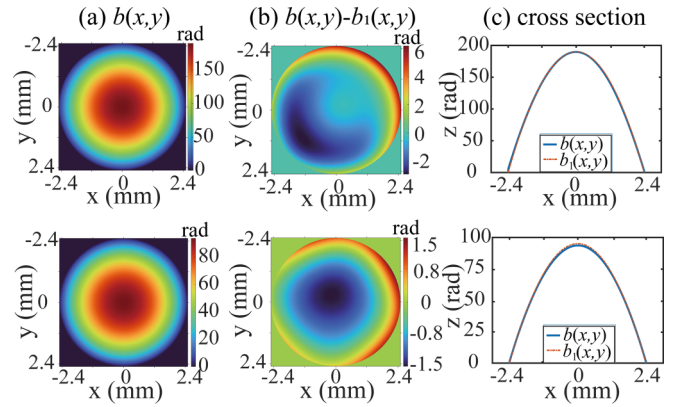


FIG. 5. Phase reconstruction for large phase gradients. The top and bottom rows correspond to lenses with focal lengths $f_1 \approx 15$ cm and $f_2 \approx 30$ cm, respectively. The x axis and y axis represent the aperture of the measured phase, and the z axis and the color bar characterize the size of the phase. (a) The reconstructed phases $b(x, y)$. (b) The reconstructed accuracy. It is the difference between the reconstructed result $b(x, y)$ and theoretical result $b_1(x, y)$. The PV and RMS values of the reconstructed accuracy corresponding to the two lenses are about 1.44λ (9.05 rad) and 0.27λ (1.70 rad), 0.50λ (3.14 rad), and 0.12λ (0.75 rad), respectively. (c) The cross sections of the reconstructed result $b(x, y)$ and theoretical result $b_1(x, y)$.

measurement to obtain the phase differentiation without using the temporal phase shifts or spatial-carrier phase shifting method. Moreover, under weak coupling, the square of the derivative of phase is obtained directly.

In summary, we have demonstrated that under weak coupling, the square of the phase derivative of the target object can be measured directly, where three weak phase distributions loaded directly into SLM are measured. However, for the wave function with large phase gradients, the phase differentiation is wrapped. The reason is that when the eigenvalues corresponding to the momentum states are all small, the probability distribution function is seen as the sum of the derivatives of each eigenstate, and when the eigenvalues are large, the probability distribution function has other implications. The wrapped phase hides the differentiation information, which requires an unwrapping algorithm to obtain phase differentiation. We experimentally measured the phase of collimated light passing through two lenses with different focal lengths. The results were as we expected, and by the unwrapping algorithm, we get the phase differentiation. Finally, combining with DZF, the measured phase is reconstructed. This work retains the advantages of weak measurement techniques and validates measurements of large phase gradients, which can extend the application of weak measurement to wavefront sensing.

[1] D. T. Smithey, M. Beck, M. G. Raymer, and A. Faridani, Measurement of the Wigner distribution and the density-matrix of a light mode using optical homodyne tomography: Application to squeezed states and the vacuum, *Phys. Rev. Lett.* **70**, 1244 (1993).

[2] G. Breitenbach, S. Schiller, and J. Mlynek, Measurement of the quantum states of squeezed light, *Nature (London)* **387**, 471 (1997).

[3] J. S. Lundeen, B. Sutherland, A. Patel, C. Stewart, and C. Bamber, Direct measurement of the

- quantum wavefunction, *Nature (London)* **474**, 188 (2011).
- [4] Y. Aharonov, D. Z. Albert, and L. Vaidman, How the result of a measurement of a component of the spin of a spin-1/2 particle can turn out to be 100, *Phys. Rev. Lett.* **60**, 1351 (1988).
- [5] J. Dressel, M. Malik, F. M. Miatto, A. N. Jordan, and R. W. Boyd, Colloquium: Understanding quantum weak values: Basics and applications, *Rev. Mod. Phys.* **86**, 307 (2014).
- [6] Z. M. Shi, M. Mirhosseini, J. Margiewicz, M. Malik, F. Rivera, Z. Y. Zhu, and R. W. Boyd, Scan-free direct measurement of an extremely high-dimensional photonic state, *Optica* **2**, 388 (2015).
- [7] M. Yang, Y. Xiao, Y.-W. Liao, Z.-H. Liu, X.-Y. Xu, J.-S. Xu, C.-F. Li, and G.-C. Guo, Zonal reconstruction of photonic wavefunction via momentum weak measurement, *Laser Photon. Rev.* **14**, 1900251 (2020).
- [8] J. Zhu, A. Wang, X. Liu, Y. Liu, Z. Zhang, and F. Gao, Reconstructing the wave function through the momentum weak value, *Phys. Rev. A* **104**, 032221 (2021).
- [9] J. Zhu, Z. Li, Y. Liu, Y. Ye, Q. Ti, Z. Zhang, and F. Gao, Weak measurement with the peak-contrast-ratio pointer, *Phys. Rev. A* **103**, 032212 (2021).
- [10] J. H. Bruning, D. R. Herriott, J. E. Gallagher, D. P. Rosenfeld, A. D. White, and D. J. Brangaccio, Digital wavefront measuring interferometer for testing optical surfaces and lenses, *Appl. Opt.* **13**, 2693 (1974).
- [11] J. P. Gardner, J. C. Mather, M. Clampin, R. Doyon, M. A. Greenhouse, H. B. Hammel, J. B. Hutchings, P. Jakobsen, S. J. Lilly, K. S. Long, J. I. Lunine, M. J. McCaughrean, M. Mountain, J. Nella, G. H. Rieke, M. J. Rieke, H. W. Rix, E. P. Smith, G. Sonneborn, M. Stiavelli *et al.*, The James Webb Space Telescope, *Space Sci. Rev.* **123**, 485 (2006).
- [12] M. J. Booth, M. A. A. Neil, R. Juskaitis, and T. Wilson, Adaptive aberration correction in a confocal microscope, *Proc. Natl. Acad. Sci. USA* **99**, 5788 (2002).
- [13] J. Porter, A. Guirao, I. G. Cox, and D. R. Williams, Monochromatic aberrations of the human eye in a large population, *J. Opt. Soc. Am. A* **18**, 1793 (2001).
- [14] K. Park, T. D. Yang, D. Seo, M. G. Hyeon, T. Kong, B.-M. Kim, Y. Choi, W. Choi, and Y. Choi, Jones matrix microscopy for living eukaryotic cells, *ACS Photon.* **8**, 3042 (2021).
- [15] K. Itoh, Analysis of the phase unwrapping algorithm, *Appl. Opt.* **21**, 2470 (1982).
- [16] R. M. Goldstein, H. A. Zebker, and C. L. Werner, Satellite radar interferometry: Two-dimensional phase unwrapping, *Radio Sci.* **23**, 713 (1988).
- [17] M. A. Herráez, D. R. Burton, M. J. Lalor, and M. A. Gdeisat, Fast two-dimensional phase-unwrapping algorithm based on sorting by reliability following a noncontinuous path, *Appl. Opt.* **41**, 7437 (2002).
- [18] X. Liu, A polarized lateral shearing interferometer and application for on-machine form error measurement of engineering surfaces, Ph.D. thesis, Hong Kong University of Science and Technology, 2003.
- [19] W. Shen, M.-W. Chang, and D.-S. Wan, Zernike polynomial fitting of lateral shearing interferometry, *Optical Engineering* **36**, 905 (1997).
- [20] A. G. Kofman, S. Ashhab, and F. Nori, Nonperturbative theory of weak pre- and post-selected measurements, *Phys. Rep.* **520**, 43 (2012).
- [21] J. X. Zhou, H. L. Qian, C.-F. Chen, J. X. Zhao, G. R. Li, Q. Y. Wu, H. L. Luo, S. C. Wen, and Z. W. Liu, Optical edge detection based on high-efficiency dielectric metasurface, *Proc. Natl. Acad. Sci. USA* **116**, 11137 (2019).
- [22] J. X. Zhou, S. K. Liu, H. L. Qian, Y. H. Li, H. L. Luo, S. C. Wen, Z. Y. Zhou, G. C. Guo, B. S. Shi, and Z. W. Liu, Metasurface enabled quantum edge detection, *Sci. Adv.* **6**, 4385 (2020).
- [23] S. Q. Liu, S. Z. Chen, S. C. Wen, and H. L. Luo, Photonic spin Hall effect: Fundamentals and emergent applications, *Opto-Electron. Sci.* **1**, 220007 (2022).
- [24] T. F. Zhu, C. Guo, J. Y. Huang, H. W. Wang, M. Orenstein, Z. C. Ruan, and S. H. Fan, Topological optical differentiator, *Nat. Commun.* **12**, 680 (2021).
- [25] S. S. He, J. X. Zhou, S. Z. Chen, W. X. Shu, H. L. Luo, and S. C. Wen, Spatial differential operation and edge detection based on the geometric spin Hall effect of light, *Opt. Lett.* **45**, 877 (2020).
- [26] N. W. M. Ritchie, J. G. Story, and R. G. Hulet, Realization of a measurement of a “weak value”, *Phys. Rev. Lett.* **66**, 1107 (1991).
- [27] N. A. Roddier, Atmospheric wave-front simulation using Zernike polynomials, *Opt. Eng.* **29**, 1174 (1990).